Received: 8 October 2018 | Revised: 28 November 2018 | Accepted: 5 December 2018
DOI: 10.1002/ardp.201800298

FULL PAPER

DPhG ARCH PHARM
Archiv der Pharmazie

Synthesis and biological evaluation of sphingosine kinase 2 inhibitors with anti-inflammatory activity

Marcela Vettorazzi[1] | Laura Vila[2,3] | Santiago Lima[4] | Lina Acosta[5] | Felipe Yépes[5] | Alirio Palma[5] | Justo Cobo[6] | Jan Tengler[7] | Ivan Malik[8] | Sergio Alvarez[1] | Patrice Marqués[2,3] | Nuria Cabedo[2,3] | María J. Sanz[2,3] | Josef Jampilek[8] | Sarah Spiegel[4] | Ricardo D. Enriz[1]

[1] Facultad de Química, Bioquímica y Farmacia, Universidad Nacional de San Luis, Instituto Multidisciplinario de Investigaciones Biológicas (IMIBIO-SL), San Luis, Argentina

[2] Department of Pharmacology, University of Valencia, Valencia, Spain

[3] Institute of Health Research INCLIVA University Clinic Hospital of Valencia, Valencia, Spain

[4] Department of Biology and Department of Biochemistry and Molecular Biology, Virginia Commonwealth University School of Medicine, Richmond, Virginia

[5] Laboratorio de Síntesis Orgánica, Escuela de Química, Universidad Industrial de Santander, Bucaramanga, Colombia

[6] Inorganic and Organic Department, University of Jaén, Jaén, Spain

[7] Medis International a.s., Bolatice, Czech Republic

[8] Faculty of Pharmacy, Department of Pharmaceutical Chemistry, Comenius University, Bratislava, Slovakia

Correspondence
Dr. Ricardo D. Enriz, Facultad de Química, Bioquímica y Farmacia, Universidad Nacional de San Luis, Instituto Multidisciplinario de Investigaciones Biológicas (IMIBIO-SL), Chacabuco 915, 5700 San Luis, Argentina.
Email: denriz@unsl.edu.ar

Funding information
Universidad Nacional de San Luis; Colombian Institute for Science and Research, Grant number: 110265842651; CONICET-Argentina; Slovak Research and Development Agency, Grant number: APVV-0516-12; SANOFI-AVENTIS Pharma Slovakia; Spanish Ministry of Economy and Competiveness, Grant numbers: SAF2014-57845R, SAF2017-89714-R, CP15/00150; Carlos III Institute of Health (ISCIII); European Regional Development Fund; Spanish Ministry of Innovation and Competitiveness

Abstract

The synthesis of inhibitors of SphK2 with novel structural scaffolds is reported. These compounds were designed from a molecular modeling study, in which the molecular interactions stabilizing the different complexes were taken into account. Particularly interesting is that 7-bromo-2-(2-phenylethyl)-2,3,4,5-tetrahydro-1,4-epoxynaphtho[1,2-*b*]azepine, which is a selective inhibitor of SphK2, does not exert any cytotoxic effects and has a potent anti-inflammatory effect. It was found to inhibit mononuclear cell adhesion to the dysfunctional endothelium with minimal impact on neutrophil–endothelial cell interactions. The information obtained from our theoretical and experimental study can be useful in the search for inhibitors of SphK2 that play a prominent role in different diseases, especially in inflammatory and cardiovascular disorders.

KEYWORDS
anti-inflammatory activity, bioassays, molecular modeling, sphingosine kinase 2 inhibitors, synthesis

1 | INTRODUCTION

Sphingosine-1-phosphate (S1P) is a bioactive sphingolipid mediator that is synthesized by two isoforms of sphingosine kinase (SphK1 and SphK2).[1,2] S1P regulates many important physiological functions; however, it also has a pathological role in autoimmune dysfunction, inflammation, cancer, and many other diseases.[3–7] Most of its actions are mediated by binding and signaling through a family of five G

protein-coupled receptors (S1PR1-5) leading to downstream signaling important in inflammation, immunity, and cancer.[8,9]

Although SphK1 and SphK2 share a high degree of homology, they differ in molecular weight, tissue distribution, and subcellular localization.[10] Specifically, SphK2 has an additional domain that shares no homology with SphK1.[11] Most of the research to date has been focused on SphK1 due to its strong link to cancer and inflammatory diseases.[12–14] The structural data reported by Wang and coworkers in 2013 on the active site of SphK1 has contributed to the understanding of its mechanism of action and development of SphK1 inhibitors.[15] Numerous inhibitors of SphK1 have been reported, including very potent ones, such as PF-543.[16] In contrast, much less is known regarding SphK2.

Attention on SphK2 increased greatly after the discovery of the immunosuppressant drug FTY720/Fingolimod. It is a prodrug that is phosphorylated *in vivo* by SphK2 to its active form FTY720-phosphate, a mimetic of S1P that modulates S1PR functions.[17] In addition, intracellular S1P generated by SphK2 is an endogenous inhibitor of histone deacetylases,[9] stabilizes telomerase[18] and in mitochondria, binds to prohibitin 2.[19] These studies indicate that SphK2 is involved in epigenetic regulation, aging, and mitochondrial respiratory complex function. Furthermore, SphK2 also regulates IL-2 pathways in T cells.[20] Therefore, it has been suggested that inhibitors of SphK2 may have therapeutic utility in inflammatory and/or autoimmune diseases.[20] However, despite these advances, much remains still unknown, regarding the physiological and pathological roles of this SphK isoenzyme. In order to better understand functions of SphK2 in autoimmune/inflammatory disease, there is a need to develop SphK2 inhibitors with selectivity over SphK1.

In contrast to SphK1, for which a wide number of inhibitors have been developed, very few potent inhibitors of SphK2 have been described and most of them only displayed moderate activity against SphK2. Moreover, the vast majority of them are not SphK2 specific, thus further complicating the interpretation of their *in vitro* and *in vivo* effects. The most well-known isotype specific inhibitors of SphK2 are: ABC294640,[21] (*R*)-FTY720-OMe,[22] K145,[23] and SLM6031434[24] one of the most potent reported up to now.

We have recently described two types of structural scaffolds for developing new SphK1 inhibitors.[25] These new compounds were obtained through virtual screening, being the most active compounds of these series (molecules **2–4** (Table 1)). Considering there are relatively few inhibitors of SphK2 reported, we were interested in determining whether some of the compounds in our screen with moderate or no activity against SphK1 would inhibit SphK2. Thus, in the current study we report the inhibitory activity on SphK2 and a molecular modeling approach that allowed us to design, synthesize, and evaluate the *in vitro* and *in vivo* effects of a new SphK2 inhibitor. Furthermore, we have also examined the potential anti-inflammatory effect of the most active compounds in this series.

2 | RESULTS AND DISCUSSION

2.1 | Evaluating SphK2 inhibitory activity

We first evaluated the SphK2-inhibitory activity of the 16 compounds selected from our previous screen of SphK1 inhibitors.[25] Synthesis and structural characterization of compounds **1–16** has been described[25,26] and their structures are shown in Table 1. SphK2 inhibitors were evaluated in a 384-well high-throughput format assay as described.[27] Of these compounds, only three showed significant SphK2 inhibitory activity: compounds **2**, **4**, and **13** (IC_{50} values lower than 200 μM) (Figure 1a).

Compound **2**, which had the highest inhibitory effect on SphK1 (IC_{50}, 12 μM), also showed the strongest inhibitory activity against SphK2 (IC_{50}, 27.8 μM). In turn compounds **4** and **13** displayed 56.8 and 140 μM inhibitory activity, respectively.

It is important to note that we have previously reported that K145 suppressed SphK2 activity with an IC_{50} of 33.7 μM,[27] which is comparable with the IC_{50} value determined with the conventional radioactive assay.[23] Thus, it is possible to consider that the inhibitory effects found for compound **2** are comparable to that reported for K145 and therefore very significant. However, to search for a new SphK2 inhibitor with a novel structural scaffold highly selective for SphK2, we next carried out a molecular modeling study using starting structures based on compounds **2**, **4**, and **13**.

The assay used for screening SphK compounds has been extensively characterized and demonstrated to reliably reproduce IC_{50}s for well-known SphK inhibitors.[27] However, in screening assays we used 50 μM K145 positive control for SphK2 inhibition. As shown in Supporting Information Figure S1, no SphK2 activity was observed under these conditions.

2.2 | Molecular modeling

We conducted a molecular simulation study to identify the critical molecular interactions between compounds **2**, **4**, and **13** with active site residues of SphK2. Since no crystal structure is currently available for SphK2, we generated a structural model of SphK2 using MODELLER,[28] a comparative protein structure modeling program, using the structure of SphK1 (*Homo sapiens*) (PDB ID: 3VZB, 3VZC, 3VZD, 4L02, 4V24) as a template.[15,29,30]

The main objective of this study was to assess the interactions that stabilize or destabilize receptor-ligand (R-L) complexes. As a reference, we also included the SphK2-isotype specific compounds K145[23] and SLM6031434[24] that are strong and selective SphK2 inhibitors. It was expected that this approach would produce a comparative analysis of different SphK2 inhibitory activities of these molecules in relation to their structural differences (Figure 2).

The molecular modeling study was conducted in three different stages. First, a docking analysis was carried out using the AutoDock program.[31] In the second stage, molecular dynamics (MD) simulations were made using the AMBER software package.[32] From the

TABLE 1 Structural features of compounds selected to evaluate SphK inhibitory effect[25]

Compounds	Structure	IC_{50} (μM) SphK1	IC_{50} (μM) SphK2
1	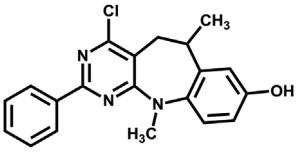	>650	>650
2	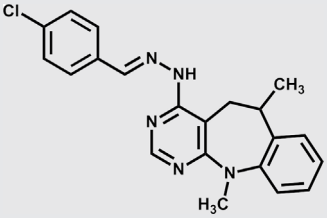	12	28
3 = −*m*-NHCOO$(CH_2)_3CH_3$	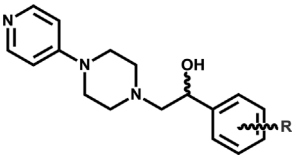	60	>650
4 = −*p*-NHCOO$(CH_2)_3CH_3$		55	57
5 = 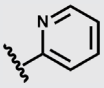	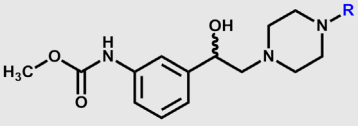	>650	>650
6 = 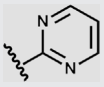		>650	>650
7 = $-CH_3$	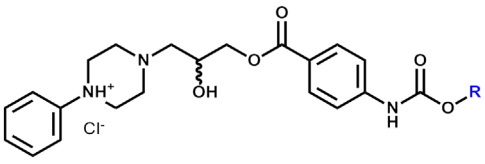	>650	>650
8 = $-CH_2CH_3$		>650	>650
9 = $-(CH_2)_3CH_3$		>650	>650
10 = R_1=$-CH_3$ R_2=$-(CH_2)_3CH_3$	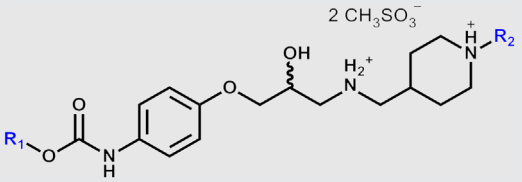	>650	>650
11 = R_1=$-(CH_2)_3CH_3$ R_2=$-(CH_2)_3CH_3$		>650	>650
12 = R_1=$-CH_3$ R_2=$-(CH_2)_2CH_3$		>650	>650
13 = R_1=$-(CH)_2CH_3$ R_2=−p-OCH_3	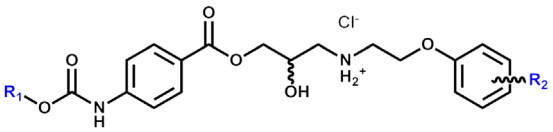	>650	140
14 = R_1=$-(CH_2)_2OCH_3$ R_2=−(2,6-dimethoxy)		>650	>650

(Continues)

TABLE 1 (Continued)

Compounds	Structure	IC_{50} (μM) SphK1	IC_{50} (μM) SphK2
15 = −o-$O(CH_2)_2OCH_3$	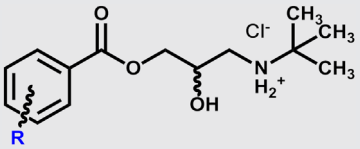	>650	>650
16 = −p-$O(CH_2)_3CH_3$		>650	>650

trajectories obtained with the MD simulations, a *per*-residue analysis was performed for each compound.

The docking analysis indicated that all compounds fit in the binding pocket of SphK2 (Figure 3). Furthermore, the docking analysis and MD simulations suggested that these compounds bind in a very comparable manner and interact with similar amino acids. Per-residue analysis helped to define the main interactions that stabilize the different complexes (Figure 4). In general, the new SphK2 inhibitors described here displayed the pharmacophoric portion at the active site in a similar manner to K145.[23]

It should be noted that SLM6031434 is more active and selective on SphK2, however, our docking studies and MD simulations indicate that this compound does not bind in a similar way to K145 nor to our compounds (Supporting Information Figure S2). Thus, for the molecular modeling studies, K145 was taken as the reference compound.

MD simulations indicate that residues participating in the stabilization of inhibitors–enzyme interactions are: Phe339, Val340, Phe358, Leu540, Leu542, Leu549, Cys569, Phe584, Met587, His592, and Leu600. Similar histograms were obtained for compounds **2**, **4** (Figure 4c and d), and **13** (Supporting Information Figure S3). It should be noted that MD simulations predicted conservation between amino acids stabilizing compounds **2**, **4**, and **13** with SphK2. Therefore, it can be concluded that these compounds bind in a similar manner to K145 as they essentially interact with the same SphK2 residues. Based on these results, we sought to obtain compounds that were structurally related to compounds **2**, **4**, and **13**, and had closely matching simulated SphK2 binding histograms.

Furthermore, it is interesting to note that compound **3** is selective for SphK1 with an IC_{50} of 60 μM, while compound **4** has an IC_{50} of 55 and 56.8 μM for SphK1 and SphK2, respectively (see Table 1). Although these compounds are isomers, our docking study shows that they are located very differently in the active site of the protein (Supporting Information Figure S4). This could give us an indication about why one is selective while the other is not.

The docking was done using the AutoDock program, using a box centered on the active site, with a size of 30 × 64 × 24 Å. Two hundred conformations were obtained, of which the lowest energy was graphed for each case.

2.3 | Design of novel SphK2 inhibitors

Several synthesizable compounds with modifications on the basic structures of compounds **2** and **13** structures were simulated in the docking analysis and MD computations. Two aspects were considered for the selection of the candidate compounds. On one hand, a

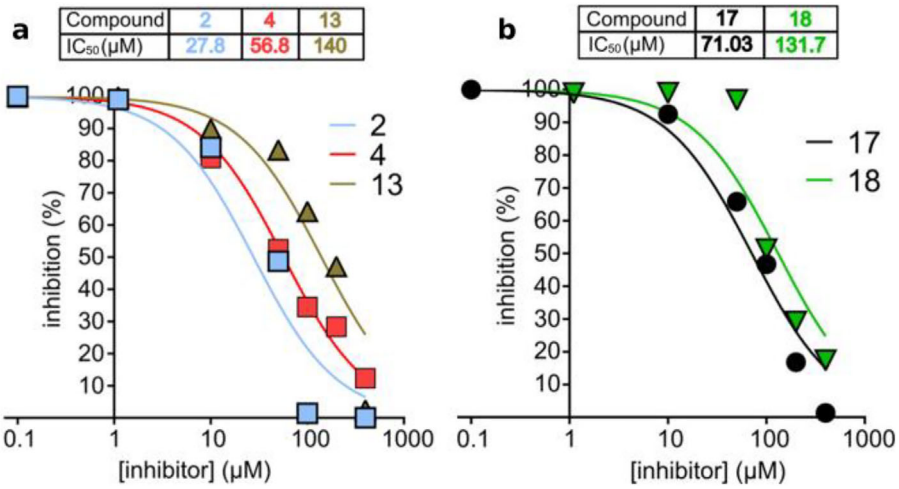

FIGURE 1 SphK2 percent inhibition versus concentration plot for the compounds **2**, **4**, **13** (a), **17** and **18** (b)

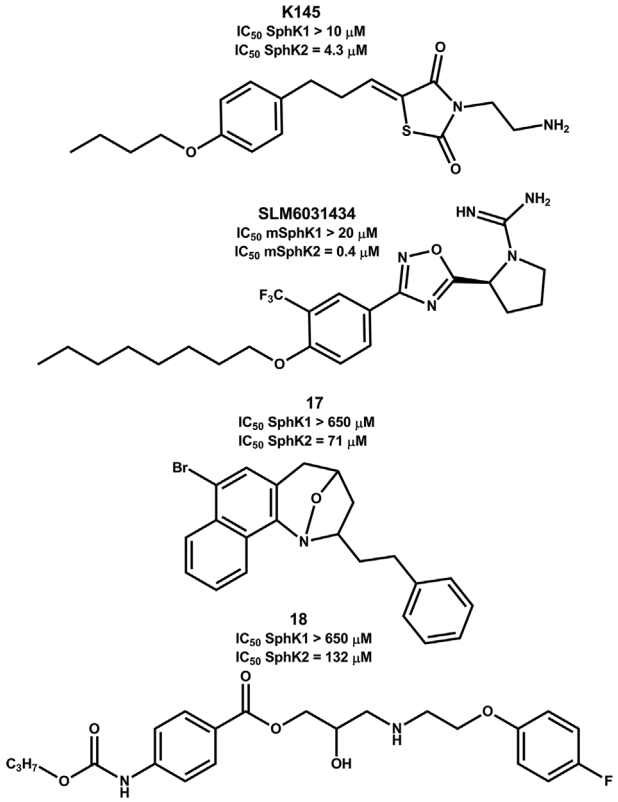

FIGURE 2 Structural features of K145, SLM6031434 and compounds **17** and **18**. mSphK1 and mSphK2 correspond to mouse sphingosine kinase 1 and 2, respectively. All other determinations were performed on human cells

limitation was that the proposed compound was available in our laboratory or that it could be synthesized without major problems for us. The other condition was that it had a certain structural similarity (at least considering its central scaffolding) with compounds **2**, **4**, and **13**.

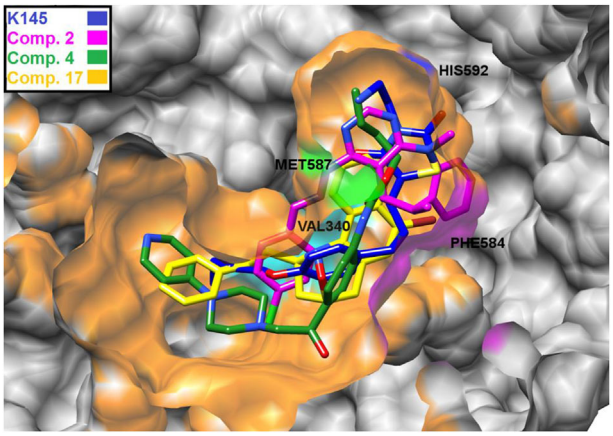

FIGURE 3 Spatial view of the overlap of the following compounds: K145 (blue), **2** (magenta), **4** (green), and **17** (yellow). These compounds are interacting in the active site of SphK2. The main amino acids involved in the formation of the complexes are also shown in this figure. The structures were taken from a clustering process in which the last 40 ns of each of the three simulations were considered

Of 12 potential SphK2 inhibitors (structures shown in Supporting Information Table S1), only 7-bromo-2-(2-phenylethyl)-2,3,4,5-tetrahydro-1,4-epoxynaphtho[1,2-*b*]azepine (**17**) and *N*-[2-(4-fluorophenoxy)ethyl]-2-hydroxy-3-({4-[(propoxycarbonyl)amino]benzoyl)-oxy)-propan-1-aminium chloride (**18**) (Figure 2) behaved similarly in our simulations as known SphK 2 inhibitors. As shown in Figures 5 and 3 (for compound **17**), SphK2-active binding site was very similar to those obtained for compounds **2**, **4** (Figure 4c and d), and **13** (Supporting Information Figure S3), as they were to the simulations with the reference compound, K145 (Figure 4a).

2.4 | Synthesis and inhibition studies for compounds 17 and 18

Compounds **17** and **18** were synthesized and evaluated for their inhibitory activity against SphK2. Compound **17** was synthesized as previously reported,[33] and involved the selective oxidation of the corresponding 2-allyl-4-bromo-*N*-(3-phenylpropyl)naphthalen-1-amine with an excess of hydrogen peroxide solution in the presence of catalytic amount of sodium tungstate. The subsequent internal 1,3-dipolar cycloaddition of the resulting nitrone toward the terminal C═C bond of the pendant allylic fragment connected to the *ortho* position gave the tricyclic 1,4-epoxycycloadduct **17** (Scheme 1). In these conditions, the thermal induced intramolecular 1,3-dipolar cycloaddition of the intermediate nitrone was entirely stereoselective leading to the exclusive formation of the 2-*exo*-cycloadduct, as demonstrated by ^{1}H NMR spectroscopy. The stereochemistry was deduced from chemical shift and coupling constant values of protons at the 1,4-epoxytetrahydroazepine ring protons (see Section 4), and especially because of the absence of correlation between tertiary 2-H and 4-H protons in the NOESY spectrum. Compound **17** was obtained as a racemic mixture of (2*R*,4*S*) and (2*S*,4*R*) forms.

N-[2-(4-Fluorophenoxy)ethyl]-2-hydroxy-3-({4-[(propoxycarbonyl)amino]benzoyl}oxy)propan-1-aminium chloride (**18**) was synthesized by the multiple-step reactions shown in Scheme 2 and described by Tengler et al.[34] Briefly, oxiran-2-ylmethyl-4-[(propoxycarbonyl)amino]benzoate was prepared from 4-aminobenzoic acid by reaction with propyl chloroformiate that yielded 4-[(propoxycarbonyl)amino]benzoic acid that was converted to propyl [4-(chlorocarbonyl)phenyl]carbamate by reaction with thionyl chloride. The desired epoxide was formed after reaction of propyl [4-(chlorocarbonyl)phenyl]carbamate with 2,3-epoxypropan-1-ol. The oxirane ring was opened by addition of 2-(4-fluorophenoxy)ethanamine prepared by Gabriel synthesis from 4-fluorophenol via 1-(2-bromoethoxy)-4-fluorobenzene and 1-(2-bromoethoxy)-4-fluorobenzene. The product, 3-{[2-(4-fluorophenoxy)ethyl]amino}-2-hydroxypropyl 4-[(propoxycarbonyl)amino]benzoate, was transformed to the hydrochloride salts with higher water solubility using ethereal HCl.

SphK2 inhibition assays were performed as previously described[27] with **17** and **18**. Compound **17** showed a higher SphK2 inhibitory capacity (71.0 μM), while compound **18** expressed only moderate activity (131.7 μM), see Figure 1b. Interestingly, compound

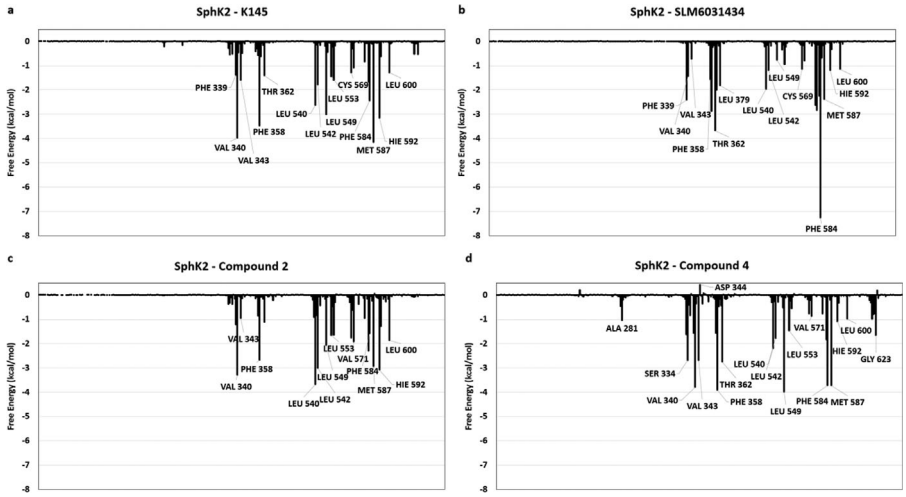

FIGURE 4 Histograms show the interaction energies obtained for the specific inhibitors K145 (a), SLM6031434 (b) and compounds **2** (c) and **4** (d) with the main amino acids involved in the complex formation

17 inhibits SphK2 but had no inhibitory effect on SphK1 (data shown in Table 1).

As it has been suggested that development of SphK1/SphK2 selective inhibitors might be useful for treatment of inflammatory and/or autoimmune diseases,[12,35] it was of interest to evaluate the potential anti-inflammatory effect of **17**. To establish proper comparisons, compounds **2**–**4** and **17** were tested. In regard to this, compound **2** was the most potent in the series, but non-isotype-selective (IC_{50} SphK1 = 12 μM and IC_{50} SphK2 = 28 μM); compound **4** inhibited both enzymes but weaker than **2** (IC_{50} SphK1 = 55 μM and IC_{50} SphK2 = 56 μM); compound **3** was selective for SphK1 (IC_{50} SphK1 = 60 μM) and compound **17** selectively inhibited SphK2 (IC_{50} SphK2 = 71 μM). Interestingly compound **17** does not show any inhibitory effect against SphK1 even at high concentration (650 μM).

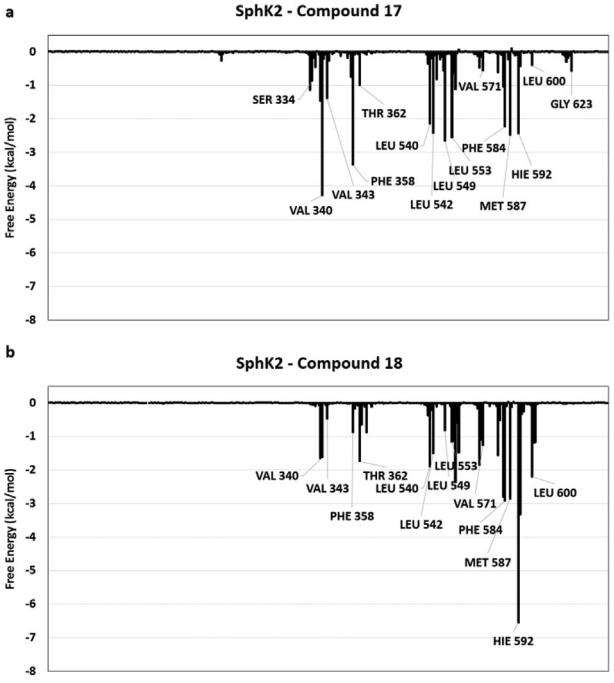

FIGURE 5 Histograms show the interaction energies obtained for **17** (a) and **18** (b) with the main amino acids involved in the complex formation

2.5 | Cell viability assay

The cytotoxicity effects of these compounds on cell viability were determined by MTT assay. Compound **2**, with a benzo[*b*]pyrimido[5,4-*f*]azepine system, showed high cytotoxicity in human umbilical vein endothelial cells (HUVEC) and human neutrophils, decreasing cell viability by more than 40% at 10 μM (Figure 6a and b).

Compound **3** with a pyridinyl-piperazine phenyl 3-carbamate structure, displayed cytotoxicity in HUVEC at 30 μM and was cytotoxic for neutrophils at all concentrations assayed (10–100 μM) (Figure 6c and d). In contrast, compound **4**, an isomer of **3**, showed no toxicity at 100 μM in HUVEC when it was compared with vehicle (0.04% DMSO in medium). Compound **17** with an epoxynaphtho[1,2-*b*]azepine system, only showed significant toxicity at the maximum dose of 100 μM in human neutrophils but cell viability remained higher than 70% (Figure 6e–h).

2.6 | Compound 17 reduces the adhesion of leukocytes to dysfunctional endothelium

Inflammation and especially the adhesion of mononuclear cell to the dysfunctional endothelium play an important role in atherosclerosis development.[36] One of the key events in the inflammatory process involves endothelial-leukocyte adhesion and their subsequent emigration to the extravascular space.[37] To examine the effect of SphK2 inhibition with the less toxic compounds **4** and **17** on leukocyte adhesion, parallel-plate flow chamber assays were carried out. This experimental setting allows studies of leukocyte–endothelial cell

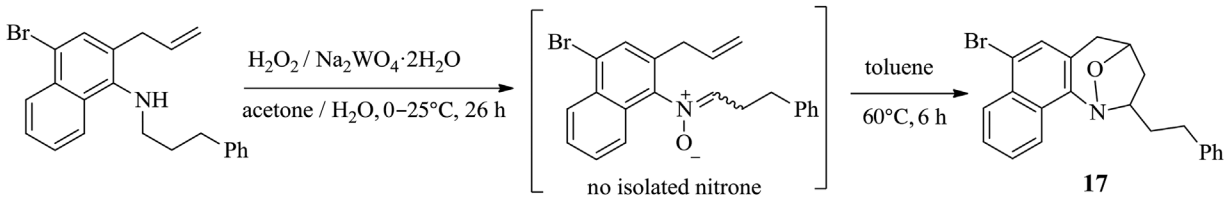

SCHEME 1 Synthesis of (2*RS*,4*SR*)-7-bromo-2-(2-phenylethyl)-2,3,4,5-tetrahydro-1,4-epoxynaphtho[1,2-*b*]azepine (**17**)

interactions under flow conditions mimicking the *in vivo* physiological fluid dynamics within the blood vessels of the microcirculation. When neutrophils were perfused across TNFα-stimulated endothelial cells, significant leukocyte adhesion was observed compared to the adhesion to unstimulated endothelial cells (0.04% DMSO, Figure 7a). Preincubation with compound **4**, the pyridinyl-piperazine phenyl 4-carbamate, prior to TNFα stimulation, did not affect TNFα-induced neutrophil adhesion to endothelial cells at the concentration assayed (100 μM, Figure 7a). When endothelial cells were incubated with compound **17**, the epoxynaphtho[1,2-*b*]azepine, although some inhibition of neutrophil arrest to the dysfunctional endothelium (TNFα stimulated) was detected, the reduction in this parameter was below 50% (43.4%) at 100 μM (Figure 7a).

Compounds **4** and **17** were firstly assayed at 100 μM to evaluate their impact on mononuclear cell adhesion. At this concentration, while compound **4** did not significantly affect TNFα-induced mononuclear cell-endothelial adhesion, compound **17** did (Figure 7b). Since this effect was inhibited by 70%, at 100 μM, the effect of compound **17** was analyzed within a concentration range of 0.1–100 μM. Interestingly, compound **17** inhibited in a concentration-dependent manner mononuclear leukocyte-endothelial cell adhesion elicited by TNFα (Figure 7c) with an estimated IC_{50} of 3 μM. These results are relevant given that the effect on mononuclear cell recruitment exerted by compound **17** differs from those displayed on neutrophils suggesting that it likely does not compromise neutrophilic responses which are necessary for innate host defence.

In order to explore the mechanisms involved in the decreased mononuclear cell adhesion to endothelial cells provoked by compound **17**, we next investigated its effect on endothelial cell adhesion molecule (CAM) expression and fractalkine (CX_3CL1) up-regulation. TNFα caused increased endothelial expression of intercellular adhesion molecule-1 (ICAM-1, Figure 8a), vascular cell adhesion molecule-1 (VCAM-1, Figure 8b), and the membrane-bound chemokine fractalkine (CX_3CL1, Figure 8c). It is interesting to point out that both VCAM-1 and fractalkine (CX_3CL1) are mainly expressed in the vasculature at sites prone to atherosclerosis lesion formation and here we show that preincubation of endothelial cells with compound **17** at 10 μM, significantly reduced TNFα-induced ICAM-1 (a), VCAM-1 (b), and fractalkine (CX_3CL1) (c) expression by 60.0, 60.2, and 59.1%, respectively (Figure 8).

In conclusion, our results indicate that compound **17** which is a SphK2 selective inhibitor, shows no (endothelial cells) or low toxicity (neutrophils) toward human cells and is able to inhibit mononuclear cell adhesion to the dysfunctional endothelium with a minimal impact on neutrophil responses. These responses are in part mediated through down-regulation of endothelial cell adhesion molecule and fractalkine expression (CX_3CL1). Therefore, compound **17** is a potential candidate to be used in the treatment of inflammatory disorders in which mononuclear cell recruitment plays a prominent role such as cardiovascular diseases associated to cardiometabolic disorders.

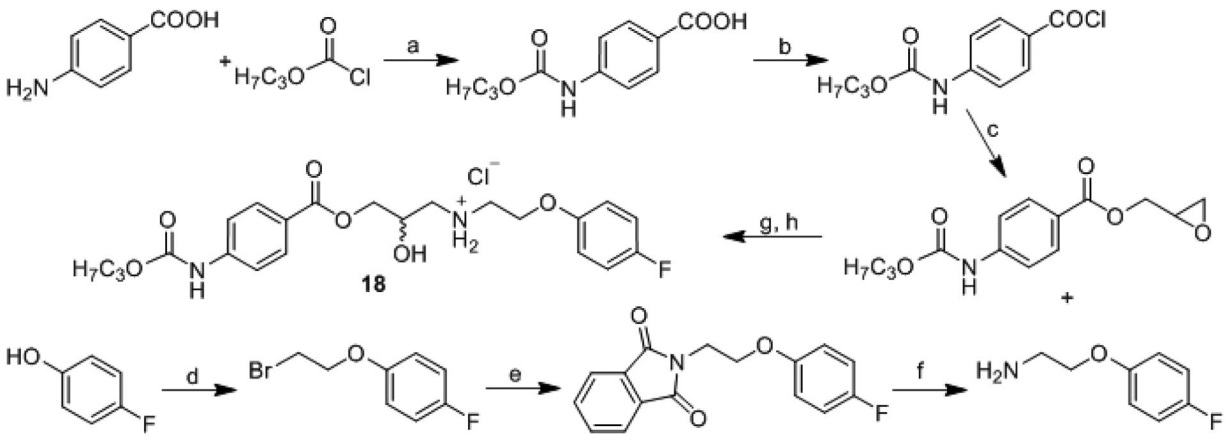

SCHEME 2 Synthesis of *N*-[2-(4-fluorophenoxy)ethyl]-2-hydroxy-3-({4-[(propoxycarbonyl)amino]benzoyl}oxy)propan-1-aminium chloride (**18**).[34] *Reagents and conditions:* a) acetone, pyridine; b) $SOCl_2$, toluene; c) 2,3-epoxypropan-1-ol, THF, TEA; d) 1,2-dibromoethane, NaOH; e) potassium phthalimide, KI, DMF; f) $NH_2NH_2.H_2O$, ethanol; g) propan-2-ol; h) HCl, Et_2O

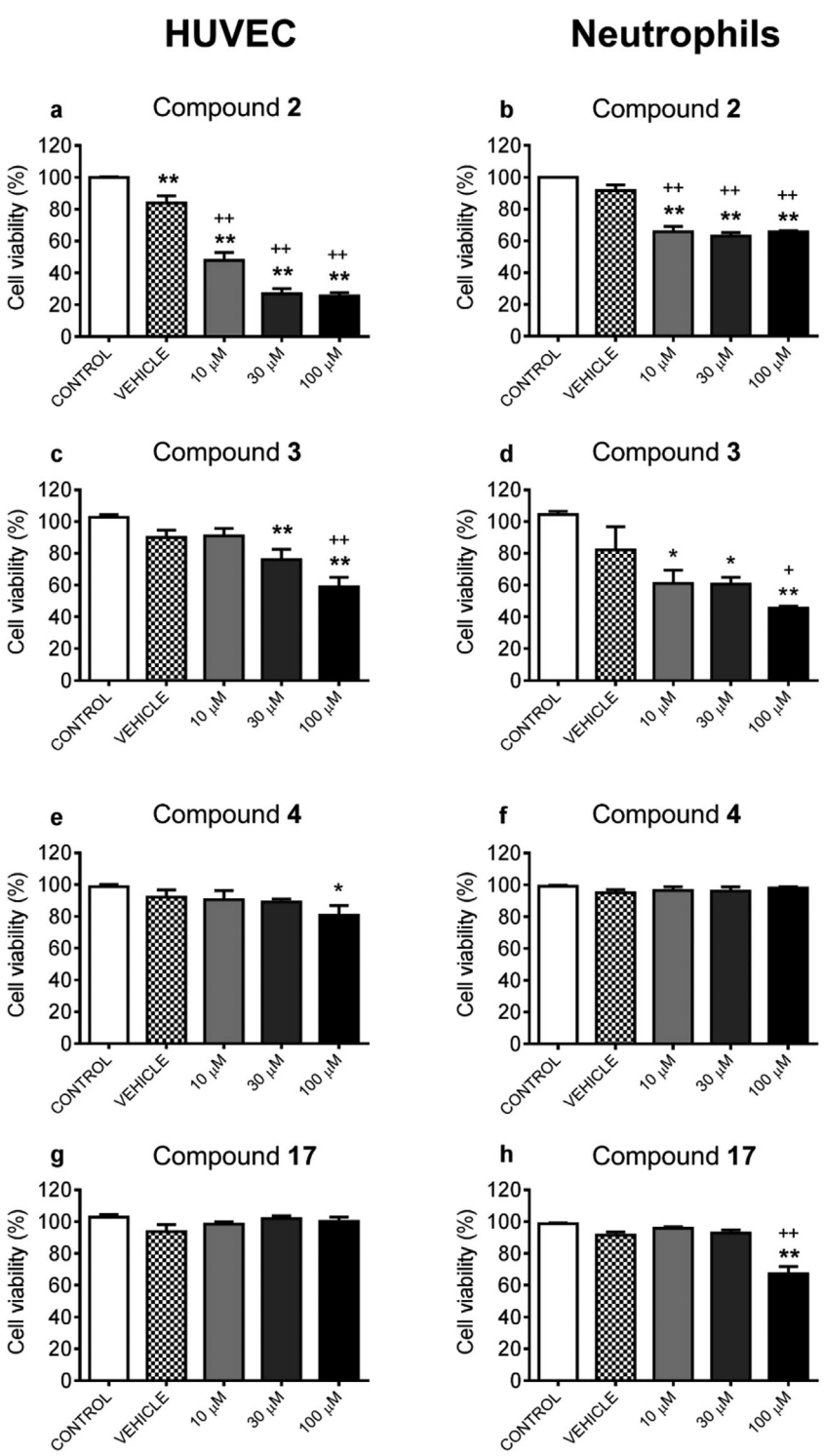

FIGURE 6 HUVEC and human neutrophil viability after 24 h incubation with four sphingosine kinase inhibitors. Cells were incubated with compounds **2**–**4** and **17** at 10, 30, and 100 μM, just with medium (control) or medium plus vehicle (vehicle, 0.04% DMSO in medium) for 24 h and MTT assay was performed. Data are presented as mean ± SEM of the percentage of viable cells in $n = 5$ independent experiments. $^{*}p < 0.05$ or $^{**}p < 0.01$ versus control, $^{+}p < 0.05$ or $^{++}p < 0.01$ versus vehicle

3 | CONCLUSIONS

In this work, we used a molecular modeling approach that allowed us to obtain new inhibitors of SphK2 with novel structural scaffolds. Particularly interesting is that compound **17** which is a selective inhibitor of SphK2 and does not have exert any cytotoxic effects, has a potent anti-inflammatory effect since it inhibits mononuclear cell adhesion to the dysfunctional endothelium.

It should be noted that compound **17** shows an anti-inflammatory activity in a concentration-dependent manner with an IC_{50} in the low micromolar range. Therefore, based on our results we cannot say that the anti-inflammatory activity of this compound is due only to the action on this enzyme. In fact, it is logical to have doubts about the mechanisms responsible to produce the anti-inflammatory effect of these compounds. However, it is reasonable to think that its biological activity is due, at least in part, to the aforementioned inhibitory effect. On the other hand, its profile makes itself an interesting starting structure for the search for new selective inhibitors of SphK2, as well as new anti-inflammatory agents.

It is important to note that 7-bromo-2-(2-phenylethyl)-2,3,4,5-tetrahydro-1,4-epoxynaphtho[1,2-*b*]azepine (**17**) was obtained from a molecular modeling study carried out based on the structure of 4-[(2*E*)-2-(4-chlorobenzylidene)hydrazinyl]-6,11-dimethyl-6,11-dihydro-5*H*-pyrimido[4,5-*b*][1]benzazepine (**2**) and using K145 as control structure. Therefore, the information obtained from this theoretical model based on the molecular interactions involved in the stabilization of the different complexes can be useful in the search for new inhibitors of SphK2 recruitment, which plays a prominent role, such in inflammatory and cardiovascular diseases.

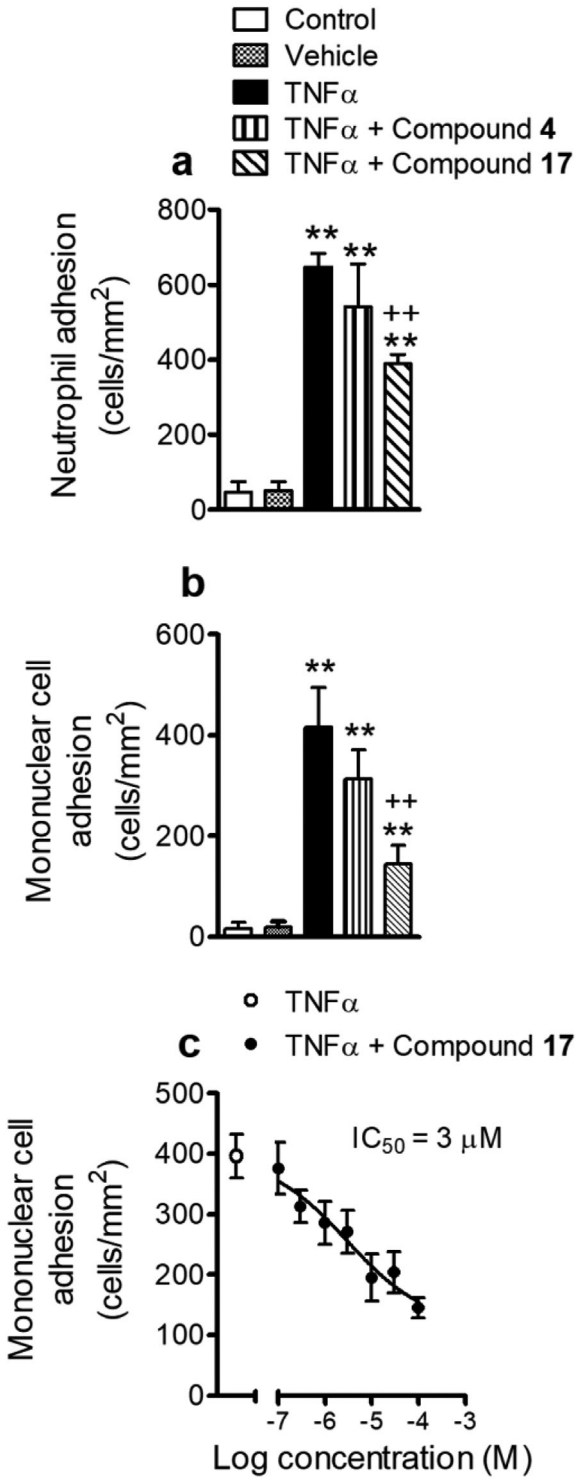

FIGURE 7 Continued.

4 | EXPERIMENTAL

4.1 | Chemistry

4.1.1 | General

Commercially available compounds were used as received, unless stated otherwise. Melting points were measured by a Barstead electrothermal 9100 apparatus or a Kofler hot plate apparatus HMK (Franz Kustner Nacht GK, Dresden, Germany) and are uncorrected. TLC was performed on silica gel 60 F_{254} on aluminum sheets (Merck, Darmstadt, Germany) and visualized with UV light (254 nm). Compounds were purified by silica gel 60 (40–63 μm, Merck 9385) column

FIGURE 7 (a) Compound **17** but not **4** modestly inhibits neutrophil adhesion to the dysfunctional endothelium (TNFα-stimulated). Cells were pretreated for 24 h with compound **4**, **17** (100 μM), just with medium (control) or medium plus vehicle (vehicle, 0.04% DMSO) prior to TNFα stimulation (20 ng/mL, 24 h). Freshly isolated human neutrophils were perfused across the endothelial monolayers for 5 min at 0.5 dynes/cm^2 and neutrophil adhesion was quantified. (b and c) Compound **17** inhibits mononuclear cell adhesion to the dysfunctional endothelium (TNFα-stimulated) in a concentration-dependent manner. (b) Cells were pretreated for 24 h with compound **4**, **17** (100 μM), just with medium (control) or medium plus vehicle (vehicle, 0.04% DMSO) prior to TNFα stimulation (20 ng/mL, 24 h). Freshly isolated human mononuclear cells were perfused across the endothelial monolayers for 5 min at 0.5 dynes/cm^2 and mononuclear cells adhesion was quantified. (c) Cells were pretreated for 24 h with compound **17** (0.1–100 μM), just with medium (control) or medium plus vehicle (vehicle, 0.04% DMSO) prior to TNFα stimulation (20 ng/mL, 24 h). Freshly isolated human mononuclear cells were perfused across the endothelial monolayers for 5 min at 0.5 dynes/cm^2 and mononuclear cell adhesion was quantified. Results are the mean ± SEM of 4–6 independent experiments. $^{**}p < 0.01$ versus vehicle, $^{++}p < 0.01$ versus TNFα-stimulated cells

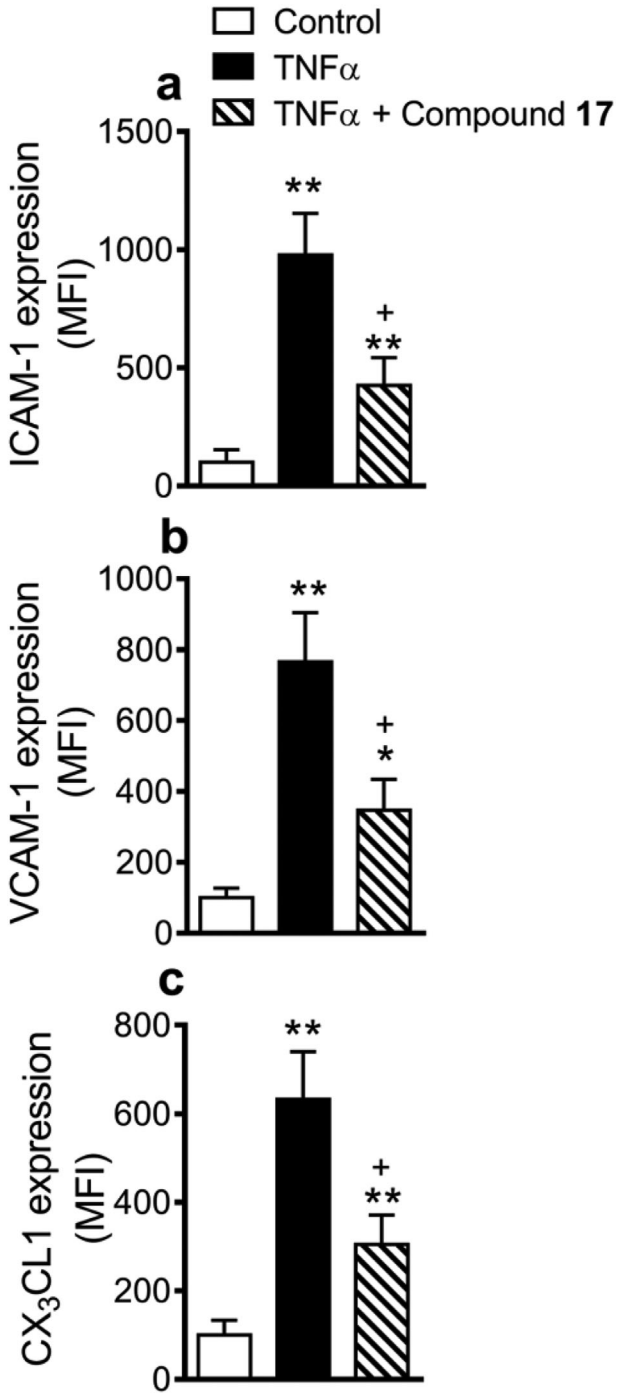

FIGURE 8 Compound **17** inhibits TNFα-induced ICAM-1, VCAM-1, and CX_3CL1 expression on HUVEC. Some cells were pretreated with compound **17** (10 μM) 24 h before TNFα stimulation (20 ng/mL, 24 h) or with vehicle (0.04% DMSO in medium). ICAM-1 (a), VCAM-1 (b), and CX_3CL1 (c) expression was determined by flow cytometry. Results (mean ± SEM) are expressed as the mean fluorescence intensity (MFI) of $n = 6$ independent experiments. $^{*}p < 0.05$ or $^{**}p < 0.01$ relative to the vehicle group, $^{+}p < 0.05$ or $^{++}p < 0.01$ relative to TNFα-stimulated cells

chromatography. ^{1}H NMR and ^{13}C NMR spectra were recorded at 25°C with $CDCl_3$, CD_3OD or DMSO-d_6 as solvents on Bruker AC-300, AC-400, AC-500 or Avance III 400 MHz FT-NMR spectrometers (Bruker, Karlsruhe, Germany). The carbon typology (C, CH, CH_2 or CH_3) was deduced from ^{13}C NMR DEPT experiments, which along with the 2D experiments, COSY, HSQC, and HMBC correlations, permitted the full assignation of all carbons and hydrogens. Chemical shifts are relative to the solvent peaks used as reference and reported in δ parts per million (ppm), and *J* values in Hz. High-resolution mass spectra (HRMS) were measured using a high-performance liquid chromatograph Dionex UltiMate® 3000 (Thermo Scientific, West Palm Beach, FL, USA) coupled with a LTQ Orbitrap XL™ Hybrid Ion Trap-Orbitrap Fourier transform mass spectrometer (Thermo Scientific) with injection into HESI II in the positive or negative mode, or on a Waters Micromass AutoSpect NT (equipped with a direct inlet probe) by electronic impact operating at 70 eV. IR spectra were recorded on a Bruker Tensor 27 spectrometer (equipped with a platinum ATR cell).

The InChI codes of the investigated compounds together with some biological activity data are provided as Supporting Information.

4.1.2 | Synthesis of (2*RS*,4*SR*)-7-bromo-2-phenethyl-2,3,4,5-tetrahydro-1,4-epoxy-naphtho[1,2-*b*]azepine (17)

Sodium tungstate dihydrate $Na_2WO_4.2H_2O$ (0.072 g, 0.22 mol), followed by 30% aqueous hydrogen peroxide solution (0.74 mL, 6.72 mmol), were added to a stirred and cooled solution of the 2-allyl-4-bromo-*N*-(3-phenylpropyl)naphthalen-1-amine (0.85 g, 2.24 mmol) in acetone–water (30 mL, 10:3 v/v). The resulting mixture was stirred at ambient temperature for 26 h, after that was filtered and the solvent removed under reduced pressure. Toluene (30 mL) was added to the organic residue and the resulting solution was heated at 60°C for 6 h. After cooling the solution to ambient temperature, the solvent was removed under reduced pressure and the crude product was purified by chromatography on silica using heptane–ethyl acetate (compositions ranged from 30:1 to 10:1 v/v) as eluent to afford **17** as a pale-yellow syrup in yield 43%. ^{1}H NMR ($CDCl_3$) δ 8.39 (dd, $J = 7.0$, 2.2 Hz, 1H, CH-11), 8.17 (dd, $J = 7.0$, 2.1 Hz, 1H, CH-8), 7.59 (td, $J = 7.0$, 2.2 Hz, 1H, CH-10), 7.54 (td, $J = 7.0$, 2.1 Hz, 1H, CH-9), 7.50 (s, 1H, CH-6), 7.29 (dd, $J = 8.2$, 1.7 Hz, 2H, CH-2″ and CH-6″), 7.28 (t, $J = 8.3$ Hz, 2H, CH-3″ and CH-5″), 7.18 (td, $J = 8.4$, 1.7 Hz, 1H, CH-4″), 4.94 (ddd, $J = 8.0$, 5.5, 2.8 Hz, 1H, CH-4), 3.48 (dd, $J = 16.9$, 5.5 Hz, 1H, CH_B-5), 3.17 (dddd, $J = 11.0$, 8.5, 5.5, 3.0 Hz, 1H, CH-2), 3.13 (ddd, $J = 13.9$, 11.0, 5.5 Hz, 1H, CH_A-2′), 2.84 (ddd, $J = 13.9$, 11.0, 5.5 Hz, 1H, CH_B-2′), 2.52 (d, $J = 16.9$ Hz, 1H, CH_A-5), 2.28 (dddd, $J = 13.6$, 11.0, 6.0, 5.5 Hz, 1H, CH_A-1′), 2.16–2.22 (m, 2H, CH_AH_B-3), 1.81 (ddt, $J = 13.6$, 11.0, 5.5 Hz, 1H, CH_B-1′). ^{13}C NMR ($CDCl_3$) δ 145.4 (C-11b), 141.8 (C-1″), 131.2 (C-6), 130.9 (C-7a), 128.8 (C-11a), 128.6 (C-2″ and C-6″), 128.5 (C-3″ and C-5″), 127.3 (C-8), 127.1 (C-10), 126.9 (C-9), 126.0 (C-4″), 122.4 (C-11), 122.3 (C-5a), 119.6 (C-7), 74.6 (C-4), 72.3 (C-2), 39.9 (C-3), 38.7 (C-1′), 35.2 (C-5), 33.7 (C-2′). HRMS (EI, 70 eV): $C_{22}H_{20}NOBr$ calcd. 393.0728 *m/z*. Found: 393.0722 *m/z*. IR (ATR, cm^{-1}): ν_{max} = 1497 (C=C), 1258 (C-N), 1043 (C-O), 990 (N-O).

4.1.3 | Synthesis of compound 18

The detailed synthetic pathway and full analytical characterization of the discussed compound **18** as well as intermediates are provided in Tengler et al.[34]

4.2 | SphK2 inhibition assays

Potential SphK2 inhibitors were evaluated with fluorescence SphK2 assays in 384-well format as described.[27] Briefly, compounds were dissolved in DMSO and initially screened at 650 μM. Candidates showing inhibition at this concentration were further characterized to obtain IC_{50}s. SphK2 activity was measured in 384-well plates (Greiner Bio-One, Frickenhausen, Germany) in buffer containing 30 mM Tris-HCl, pH 7.4, 0.05% Triton X-100, 200 mM KCl, and 10% glycerol, in the presence of NBD-sphingosine (60 μM; Avanti Polar Lipids), and recombinant SphK2 (15 nM). Reactions were initiated with the addition of an ATP–Mg mixture (1 mM ATP, 2 mM $MgCl_2$, 40 mM Tris-HCl pH 7.4), and followed in a TECAN Infinite M1000 fluorescence plate reader (Männedorf, Switzerland) at 37°C. Excitation and emission wavelengths were 550 and 584 nm, respectively. All data were analyzed using GraphPad Prism (La Jolla, CA, USA)

4.3 | Toxicological studies and study of potential anti-inflammatory activity

4.3.1 | Human studies

All research with human samples in the current study complied with the principles outlined in the Declaration of Helsinki and was approved by the Institutional Ethics Committee of the University Clinic Hospital of Valencia (Valencia, Spain). Written, informed consent was obtained from all volunteers.

4.3.2 | Reagents and compounds

3-(4,5-Dimethylthiazol-2-yl)-2,5-diphenyltetrazolium bromide (MTT) and dimethyl sulfoxide (DMSO) and tumor necrosis factor-alpha (TNFα) were purchased from Sigma–Aldrich (Madrid, Spain). All tested compounds **2–4** and **17** were dissolved in culture medium containing DMSO (0.04%).

4.3.3 | Cell culture

Human umbilical vein endothelial cells (HUVEC) were isolated by collagenase treatment[38] and maintained in human specific endothelial basal medium (EBM-2, Lonza, Verviers, Belgium), supplemented with endothelial growth media (EGM-2, Lonza, Verviers, Belgium) and 10% of fetal bovine serum (FBS, Lonza, Verviers, Belgium). Cells up to passage 1 were grown to confluence to preserve endothelial features. Prior to every experiment, cells were incubated 16 h in medium containing 1% FBS.

4.3.4 | MTT assay

Cytotoxicity studies were performed with both HUVECs and freshly isolated human neutrophils using 3-(4,5-dimethylthiazol-2-yl)-2,5-diphenyltetrazolium bromide (MTT) colorimetric assay.[39] Neutrophils were obtained from buffy coats of healthy donors by Ficoll-Hypaque density gradient centrifugation as described.[40] A total of 100 μL of neutrophils and HUVEC suspension in supplemented RPMI medium (2×10^5 cells/mL (Biowest, Nuaillé, France) were added to each well of a 96-well microtiter plate. Cells were incubated in the absence or presence of compounds at 37°C for 24 h. Compounds **2–4** and **17** were tested at three different concentrations: 10, 30, and 100 μM. Some assays were carried out just with medium and others with vehicle (0.04% DMSO in medium). MTT was freshly prepared at 2 mg/mL in PBS. A total of 100 μL of MTT solution was added to each well and incubated at 37°C for another 3 h. The supernatants were discarded and 200 μL of DMSO were added to each well to dissolve the formazan. The optical densities at dual wavelengths (560 and 630 nm) were determined in a spectrophotometer (Infinite M200, Tecan, Mannedorf, Switzerland). Results were presented as mean ± standard errors of mean (SEM).

4.3.5 | Leukocyte–endothelial cell interactions under flow conditions

HUVECs up to passage 1 were grown to confluence and stimulated with recombinant human TNFα (20 ng/mL) for 24 h. Cells were pre-incubated for 24 h with compounds **4** or **17** at 100 μM. Some assays were carried out just with medium or with vehicle (0.04% DMSO in medium). Then, cells were stimulated with TNFα (20 ng/mL) for another 24 h. In another set of experiments, cells were pretreated or not with compound **17** (0.1–100 μM) for 24 h prior to TNFα stimulation (20 ng/mL, 24 h). Human neutrophils and mononuclear cells were obtained from buffy coats of healthy donors by Ficoll-Hypaque density gradient centrifugation.[40] The Glycotech flow chamber (GlycoTech, Gaithersburg, MD) was assembled and placed on an inverted microscope stage. Freshly isolated neutrophils or mononuclear cells (1×10^6 cells/mL) were then perfused across the endothelial monolayers (HUVEC) unstimulated or stimulated with 20 ng/mL of TNFα for 24 h. Leukocyte interactions were determined after 5 min at 0.5 dyn/cm^2. Cells interacting on the surface of the endothelium were visualized and recorded (×20 objective, ×10 eyepiece) using phase-contrast microscope (Axio Observer A1 Carl Zeiss microscope, Thornwood, NY).

4.3.6 | Determination of cell adhesion molecule and fractalkine (CX_3CL1) expression by flow cytometry

HUVEC expression of intercellular adhesion molecule-1 (ICAM-1), vascular cell adhesion molecule-1 (VCAM-1), and fractalkine (CX_3CL1) were determined by flow cytometry. Cells were pretreated for 24 h with compound **17** (10 μM) or vehicle (0.04% DMSO in medium) and stimulated for additional 24 h with TNFα (20 ng/mL). Then, endothelial

cells were detached from culture flasks by scraping in ice-cold PBS containing 2 mM EDTA. Next, cells were washed and incubated at 2×10^6 cells/mL for 1 h at 4°C in the dark with FITC-conjugated mAb against human ICAM-1 (diluted 1:25; 400 µg/mL; clone HA58, BioLegend, San Diego, CA), an APC-conjugated mAb against human VCAM-1 (diluted 1:30; 100 µg/mL; clone STA, BioLegend, San Diego, CA) or with a PE–conjugated mAb against human CX_3CL1 (diluted 1:25; 1.25 µg/mL; clone 51637, R&D Systems, Minneapolis, MN), all diluted in PBS with 3% BSA. Samples were run in a flow cytometer (FACSVerse, BD Biosciences, San Jose, CA). The expression of ICAM-1 (FITC-fluorescence), VCAM-1 (APC-fluorescence) and CX_3CL1 (PE-fluorescence) was expressed as the mean of fluorescence intensity (MFI).

4.4 | Molecular modeling

4.4.1 | Homology modeling

Since no crystal structure is currently available for SphK2, we generated a structural model of SphK2 using MODELLER,[28] using the structure of sphingosine kinase 1 (*Homo sapiens*) (PDB ID: 3VZB, 3VZC, 3VZD, 4L02, 4V24) as a template.[15,29,30] A high degree overall homology to the template (52% in aligned regions) was found and there is a considerable sequence and structural similarity at the sphingosine binding (C4) domain.

Human SphK2 (code: Q9NRA0) sequence was obtained from the UNIPROT database (www.uniprot.org/). A position specific iterated BLAST[41,42] search against the database of Protein Data Bank proteins identified a kinase – sphingosine kinase 1 from *Homo sapiens* (PDB ID: 4V24), as the closest match to both proteins with 52.12% identity and 44% homology in the aligned regions of SphK. Unaligned regions in the protein were deleted. The model for the protein with the lowest DOPE (discrete optimized protein energy) scores was chosen for further refinement.

We refined the geometry by performing molecular dynamics simulations. The modeled protein was soaked in truncated octahedral periodic boxes of explicit water using the TIP3P model and subjected to MD simulation. All MD simulations were performed with the Amber software package. Sodium ions were added to neutralize the charge of the system. The entire system was subjected to energy minimization.

In the next place each system was then heated in the NVT ensemble from 0 to 300 K in 500 ps and equilibrated at an isothermal isobaric (NPT) ensemble for another 2 ns. A Langevin thermostat was used for temperature coupling with a collision frequency of 1.0 ps^{-1}. The particle mesh Ewald (PME) method was employed to treat the long-range electrostatic interactions in a periodic boundary condition. The SHAKE method was used to constrain hydrogen atoms. The time step for all MD is 2 fs, with a direct-space, non-bonded cutoff of 8 Å. Finally, three MD simulations of 50 ns were conducted under different starting velocity distribution functions; thus, in total 150 ns were simulated.

4.4.2 | Molecular docking

AutoDock4[31] was used to dock each compound to the SphK2 active site using a Lamarckian genetic algorithm with pseudo-Solis and Wets local search.[43] The following parameters were used: the initial population of trial ligands was constituted by 200 individuals; the maximum number of generations was set to 2.7×10^4. The maximum number of energy evaluations was 25.0×10^6. For each docking job, 200 conformations were generated. All other run parameters were maintained at their default setting. The resulting docked conformations were clustered into families by considering the backbone rmsd. The lowest docking-energy conformation was considered the most favorable orientation.[44]

4.4.3 | MD simulations

The complex geometries from docking were soaked in boxes of explicit water using the TIP3P model[45] and subjected to MD simulation. All MD simulations were performed with the Amber software package[32] using periodic boundary conditions and octahedral simulation cells. The particle mesh Ewald method (PME)[46] was applied using a grid spacing of 1.2 Å, a spline interpolation order of 4 and a real space direct sum cutoff of 10 Å. The SHAKE algorithm was applied allowing for an integration time step of 2 fs. MD simulations were carried out at 310 K temperature. Three MD simulations of 50 ns were conducted for each system under different starting velocity distribution functions; thus, in total 150 ns were simulated for each complex. The NPT ensemble was employed using Berendsen coupling to a baro/thermostat (target pressure 1 atm, relaxation time 0.1 ps). Post-MD analysis was carried out with program PTRAJ.

4.4.4 | Binding energy calculations

The MM-GBSA protocol was applied to each MD trajectory in order to calculate the relative binding energies of the SphK2-ligand complexes. The MM-GBSA method was used in a hierarchical strategy, and the details of this method have been presented elsewhere.[47] This protocol was applied to 4000 equidistant snapshots extracted from the last 40.0 ns and was used within the one-trajectory approximation. Briefly, the binding free energy (ΔG_{bind}) resulting from the formation of a RL complex between a ligand (L) and a receptor (R) is calculated as follows:

$$\Delta G_{bind} = \Delta E_{MM} + \Delta G_{sol} - T\Delta S \quad (1)$$

$$\Delta E_{MM} = \Delta E_{internal} + \Delta E_{electrostatic} + \Delta E_{vdW} \quad (2)$$

$$\Delta G_{sol} = \Delta G_{PB} + \Delta G_{SA} \quad (3)$$

where ΔE_{MM}, ΔG_{sol}, and $-T\Delta S$ are the changes in the gas-phase MM energy, the solvation free energy, and the conformational entropy

upon binding, respectively. ΔE_{MM} includes $\Delta E_{internal}$ (bond, angle, and dihedral energies), $\Delta E_{electrostatic}$ (electrostatic), and ΔE_{vdw} (van der Waals) energies. ΔG_{solv} is the sum of electrostatic solvation energy (polar contribution), ΔG_{PB}, and the non-electrostatic solvation component (nonpolar contribution), ΔG_{SA}. Polar contribution is calculated using the PB model, while the nonpolar energy is estimated by solvent accessible surface area.

ACKNOWLEDGMENTS

Grants from Universidad Nacional de San Luis (UNSL-Argentina) and Colombian Institute for Science and Research (Grant No. 110265842651) partially supported this work. Marcela Vettorazzi thanks a doctoral fellowship of CONICET-Argentina. This study was also partially supported by the Slovak Research and Development Agency (Grant No. APVV-0516-12) and by SANOFI-AVENTIS Pharma Slovakia. This work was also supported by grants SAF2014-57845R and SAF2017-89714-R, and the CP15/00150 from the Spanish Ministry of Economy and Competiveness, the Carlos III Institute of Health (ISCIII), and the European Regional Development Fund. Pre-doctoral grants: PM (FPI) from the Spanish Ministry of Innovation and Competitiveness.

CONFLICT OF INTEREST

The authors have declared no conflict of interest.

ORCID

Ricardo D. Enriz http://orcid.org/0000-0002-4846-9452

REFERENCES

[1] H. Liu, M. Sugiura, V. E. Nava, L. C. Edsall, K. Kono, S. Poulton, S. Milstien, T. Kohama, S. Spiegel, *J. Biol. Chem*. **2000**, *275*(26), 19513.
[2] T. Kohama, A. Olivera, L. Edsall, M. M. Nagiec, R. Dickson, S. Spiegel, *J. Biol. Chem*. **1998**, *273*, 23722.
[3] N. C. Hait, A. Maiti, *Mediators Inflamm*. **2017**, *2017*, 4806541.
[4] S. Spiegel, S. Milstien, *Nat. Rev. Immunol*. **2011**, *11*, 403.
[5] J. Tsuchida, M. Nagahashi, K. Takabe, T. Wakai, *Mediators Inflamm*. **2017**, *2017*, 2076239.
[6] S. Mohammed, K. B. Harikumar, *Front. Immunol*. **2017**, *8*, 296.
[7] T. Rohrbach, M. Maceyka, S. Spiegel, *Crit. Rev. Biochem. Mol. Biol*. **2017**, *52*(5), 543.
[8] K. Takabe, S. W. Paugh, S. Milstien, S. Spiegel, *Pharmacol. Rev*. **2008**, *60*(2), 181.
[9] N. C. Hait, J. Allegood, M. Maceyka, G. M. Strub, K. B. Harikumar, S. K. Singh, C. Luo, R. Marmorstein, T. Kordula, S. Milstien, S. Spiegel, *Science* **2009**, *325*(5945), 1254.
[10] D. Siow, B. Wattenberg, *Crit. Rev. Biochem. Mol. Biol*. **2011**, *46*(5), 365.
[11] A. S. Don, H. Rosen, *Biochem. Biophys. Res. Commun*. **2009**, *380*(1), 87.
[12] D. Shida, K. Takabe, D. Kapitonov, S. Milstien, S. Spiegel, *Curr. Drug Targets* **2008**, *9*, 662.
[13] P. Bouquerel, C. Gstalder, D. Müller, J. Laurent, L. Brizuela, R. A. Sabbadini, B. Malavaud, S. Pyronnet, Y. Martineau, I. Ader, O. Cuvillier, *Oncogenesis* **2016**, *5*, e209.
[14] S. S. L. Tan, L. W. Khin, L. Wong, B. Yan, C. W. Ong, A. Datta, M. Salto-Tellez, Y. Lam, C. T. Yap, *Clin. Transl. Gastroenterol*. **2014**, *5*, e51.
[15] Z. Wang, X. Min, S.-H. Xiao, S. Johnstone, W. Romanow, D. Meininger, H. Xu, J. Liu, J. Dai, S. An, S. Thibault, N. Walker, *Structure* **2013**, *21*(5), 798.
[16] M. E. Schnute, M. D. McReynolds, T. Kasten, M. Yates, G. Jerome, J. W. Rains, T. Hall, J. Chrencik, M. Kraus, C. N. Cronin, M. Saabye, M. Highkin, R. Broadus, S. Ogawa, K. Cukyne, L. Zawadzke, V. Peterkin, K. Iyanar, J. Scholten, J. Wendling, H. Fujiwara, O. Nemirovskiy, A. Wittwer, M. Nagiec, *Biochem. J*. **2012**, *444*(1), 79.
[17] V. Brinkmann, A. Billich, T. Baumruker, P. Heining, R. Schmouder, G. Francis, S. Aradhye, P. Burtin, *Nat. Rev. Drug Discov*. **2010**, *9*(11), 883.
[18] S. Panneer Selvam, R. M. De Palma, J. J. Oaks, N. Oleinik, Y. K. Peterson, R. V Stahelin, E. Skordalakes, S. Ponnusamy, E. Garrett-Mayer, C. D. Smith, B. Ogretmen, *Sci. Signal*. **2015**, *8*(381), ra58.
[19] G. M. Strub, M. Paillard, J. Liang, L. Gomez, J. C. Allegood, N. C. Hait, M. Maceyka, M. M. Price, Q. Chen, D. C. Simpson, T. Kordula, S. Milstien, E. Lesnefsky, S. Spiegel, *FASEB J*. **2011**, *25*(2), 600.
[20] E. T. Samy, C. A. Meyer, P. Caplazi, C. L. Langrish, J. M. Lora, H. Bluethmann, S. L. Peng, *J. Immunol*. **2007**, *179*(9), 5644.
[21] J. Yang, C. Yang, S. Zhang, Z. Mei, M. Shi, S. Sun, L. Shi, Z. Wang, Y. Wang, Z. Li, C. Xie, *Cancer Biol. Ther*. **2015**, *16*(8), 1194.
[22] K. G. Lim, C. Sun, R. Bittman, N. J. Pyne, S. Pyne, *Cell. Signal*. **2011**, *23*(10), 1590.
[23] K. Liu, T. L. Guo, N. C. Hait, J. Allegood, H. I. Parikh, W. Xu, G. E. Kellogg, S. Grant, S. Spiegel, S. Zhang, *PLoS ONE* **2013**, *8*(2), e56471.
[24] Y. Kharel, E. A. Morris, M. D. Congdon, S. B. Thorpe, J. L. Tomsig, W. L. Santos, K. R. Lynch, *J. Pharmacol. Exp. Ther*. **2015**, *355*(1), 23.
[25] M. Vettorazzi, E. Angelina, S. Lima, T. Gonec, J. Otevrel, P. Marvanova, T. Padrtova, P. Mokry, P. Bobal, L. M. Acosta, L. Acosta, A. Palma, J. Cobo, J. Bobalova, J. Csollei, I. Malik, S. Alvarez, S. Spiegel, J. Jampilek, R. Enriz, *Eur. J. Med. Chem*. **2017**, *139*, 461.
[26] L. Stanzel, I. Malík, P. Mokrý, *Dhaka Univ. J. Pharm. Sci*. **2016**, *15*(2), 235.
[27] S. Lima, S. Milstien, S. Spiegel, *J. Lipid Res*. **2014**, *55*(7), 1525.
[28] A. Sali, T. L. Blundell, *J. Mol. Biol*. **1993**, *234*(3), 779.
[29] J. Wang, S. Knapp, N. J. Pyne, S. Pyne, J. M. Elkins, *ACS Med. Chem. Lett*. **2014**, *5*(12), 1329.
[30] D. J. Gustin, Y. Li, M. L. Brown, X. Min, M. J. Schmitt, M. Wanska, X. Wang, R. Connors, S. Johnstone, M. Cardozo, A. Cheng, S. Jeffries, B. Franks, S. Li, S. Shen, M. Wong, H. Wesche, G. Xu, T. Carlson, M. Plant, K. Morgenstern, K. Rex, J. Schmitt, A. Coxon, N. Walker, F. Kayser, Z. Wang, *Bioorg. Med. Chem. Lett*. **2013**, *23*(16), 4608.
[31] G. M. Morris, R. Huey, W. Lindstrom, M. F. Sanner, R. K. Belew, D. S. Goodsell, A. J. Olson, *J. Comput. Chem*. **2009**, *30*(16), 2785.
[32] D. A. Case, V. Babin, J. T. Berryman, R. M. Betz, Q. Cai, D. S. Cerutti, T. E. Cheatham, T. A. Darden, R. E. Duke, H. Gohlke, A. W. Goetz, S. Gusarov, N. Homeyer, P. Janowski, J. Kaus, I. Kolossváry, A. Kovalenko, T. S. Lee, S. LeGrand, T. Luchko, R. Luo, B. Madej, K. M. Merz, F. Paesani, D. R. Roe, A. Roitberg, C. Sagui, R. Salomon-Ferrer, G. Seabra, C. L. Simmerling, W. Smith, J. Swails, R. C. Walker, J. Wang, R. M. Wolf, X. Wu, P. A. Kollman, *{Amber 14} OR − University of California, San Francisco* **2014**.
[33] S. Gómez Ayala, E. Stashenko, A. Palma, A. Bahsas, J. Amaro-Luis, *Synlett* **2006**, *14*, 2275.
[34] J. Tengler, I. Kapustíková, M. Peško, R. Govender, S. Keltošová, P. Mokrý, P. Kollár, J. ÓMahony, A. Coffey, K. Kráľová, J. Jampílek, *Sci. World J*. **2013**, *2013*, 274570.
[35] D. Plano, S. G. Amin, A. Sharma, *J. Med. Chem*. **2014**, *57*, 5509.
[36] U. Landmesser, B. Hornig, H. Drexler, *Circulation* **2004**, *109*(21 Suppl 1), II27.
[37] E. C. Butcher, *Cell* **1991**, *67*(6), 1033.
[38] C. Rius, C. Company, L. Piqueras, J. M. Cerda-Nicolas, C. Gonzalez, E. Servera, A. Ludwig, E. J. Morcillo, M.J. Sanz, *Thorax* **2013**, *68*(2), 177.
[39] M. Iacobini, A. Menichelli, G. Palumbo, G. Multari, B. Werner, D. Del Principe, *Biochem. Pharmacol*. **2001**, *61*(8), 1033.

[40] T. Mateo, Y. Naim Abu Nabah, M. Losada, R. Estelles, C. Company, B. Bedrina, J. M. Cerda-Nicolas, S. Poole, P. J. Jose, J. Cortijo, E. J. Morcillo, M. J. Sanz, *Blood* **2007**, *110*(6), 1895.
[41] S. F. Altschul, T. L. Madden, A. A. Schaffer, J. Zhang, Z. Zhang, W. Miller, D. J. Lipman, *Nucl. Acids Res*. **1997**, *25*(17), 3389.
[42] S. F. Altschul, J. C. Wootton, E. M. Gertz, R. Agarwala, A. Morgulis, A. A. Schaffer, Y.-K. Yu, *FEBS J*. **2005**, *272*(20), 5101.
[43] G. M. Morris, D. S. Goodsell, R. S. Halliday, R. Huey, W. E. Hart, R. K. Belew, A. J. Olson, *J. Comput. Chem*. **1998**, *19*(14), 1639.
[44] T. J. A. Ewing, I. D. Kuntz, *J. Comput. Chem*. **1997**, *18*(9), 1175.
[45] P. Mark, L. Nilsson, *J. Phys. Chem. A* **2001**, *105*(43), 9954.
[46] T. Darden, D. York, L. Pedersen, *J. Chem. Phys*. **1993**, *98*(12), 10089.
[47] P. A. Kollman, I. Massova, C. Reyes, B. Kuhn, S. Huo, L. Chong, M. Lee, T. Lee, Y. Duan, W. Wang, O. Donini, P. Cieplak, J. Srinivasan, D. A. Case, T. E. Cheatham, *Acc. Chem. Res*. **2000**, *33*(12), 889.

SUPPORTING INFORMATION

Additional supporting information may be found online in the Supporting Information section at the end of the article.

How to cite this article: Vettorazzi M, Vila L, Lima S, et al. Synthesis and biological evaluation of sphingosine kinase 2 inhibitors with anti-inflammatory activity. *Arch Pharm Chem Life Sci*. 2019;1–14.
https://doi.org/10.1002/ardp.201800298